Gold Nanoparticle Silica Nanopeapods

Vu Thanh Cong,[†,‡] Erdene-Ochir Ganbold,[§] Joyanta K. Saha,[∥] Joonkyung Jang,[∥] Junhong Min,[⊥] Jaebum Choo,[∇] Sehun Kim,[#] Nam Woong Song,[○] Sang Jun Son,*,[†,‡] Sang Bok Lee,*,[◆] and Sang-Woo Joo*,[§]

[†]Department of Chemistry, Gachon University, Seongnam, 461-701, Korea

[‡]Gachon Medical Research Institute, Gil Medical Center, Inchon, 405-760, Korea

[§]Department of Chemistry, Soongsil University, Seoul 156-743, Korea

[∥]Department of Nanomaterials Engineering, Pusan National University, Miryang 627-706, Korea

[⊥]School of Integrative Engineering, Chung-Ang University, Seoul 156-756 Korea

[∇]Department of Bionano Technology, Hanyang University, Sa-1-dong 1271, Ansan 426-791, Korea

[#]Molecular-level Interface Research Center and Department of Chemistry, KAIST, Daejeon, 305-701, Korea

[○]Center for Nano-Bio Convergence Research, Korea Research Institute of Standards and Science, 209 Gajeong-Ro, Yuseong-Gu, Daejeon 305-340, Korea

[◆]Department of Chemistry and Biochemistry, University of Maryland, College Park, Maryland 20742, United States

Ⓢ *Supporting Information*

ABSTRACT: A subnanometer gap-separated linear chain gold nanoparticle (AuNP) silica nanotube peapod (SNTP) was fabricated by self-assembly. The geometrical configurations of the AuNPs inside the SNTPs were managed in order to pose either a single-line or a double-line nanostructure by controlling the diameters of the AuNPs and the orifice in the silica nanotubes (SNTs). The AuNPs were internalized and self-assembled linearly inside the SNTs by capillary force using a repeated wet−dry process on a rocking plate. Transmission electron microscopy (TEM) images clearly indicated that numerous nanogap junctions with sub-1-nm distances were formed among AuNPs inside SNTs. Finite-dimension time domain (FDTD) calculations were performed to estimate the electric field enhancements. Polarization-dependent surface-enhanced Raman scattering (SERS) spectra of bifunctional aromatic linker *p*-mercaptobenzoic acid (*p*-MBA)-coated AuNP-embedded SNTs supported the linearly aligned nanogaps. We could demonstrate a silica wall-protected nanopeapod sensor with single nanotube sensitivity. SNTPs have potential application to intracellular pH sensors after endocytosis in mammalian cells for practical purposes. The TEM images indicated that the nanogaps were preserved inside the cellular constituents. SNTPs exhibited superior quality SERS spectra in vivo due to well-sustained nanogap junctions inside the SNTs, when compared to simply using AuNPs without any silica encapsulation. By using these SNTPs, a robust intracellular optical pH sensor could be developed with the advantage of the sustained nanogaps, due to silica wall-protection.
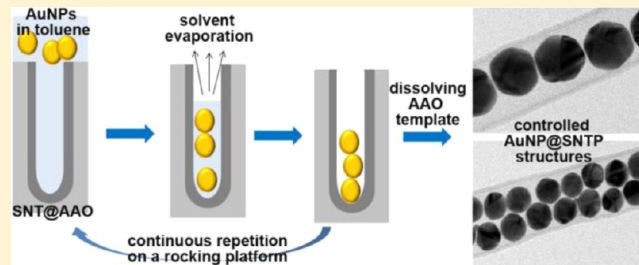
INTRODUCTION

Ordered arrays of metal nanoparticles hold great promise for many applications.[1] The successful synthesis of a one-dimensional hybrid nanosystem, known as a "peapod" offers a promising opportunity to realize a wide variety of function-alities.[2] Despite several reports[3,4] on the encapsulation of metal nanoparticles, there has been no report on self-aligned subnanometer gap fabrication by controlling the single-line and double-line configuration inside silica tubes.

Over the past several decades, nanogap-separated metal array has been a subject of great interest in plasmonic engineering.[5] Extremely strong electric fields can be formed in the gap between the noble metal nanoparticles (NPs), when they are brought closer together than a few nanometers.[6−9] Among the applications of the closely approached metal NPs, surface-enhanced Raman scattering (SERS) has been newly born as a promising method by which to detect a trace amount of surface adsorbates in an extremely sensitive way.[10−12] A spatial confinement of plasmonic NPs leads to the detection of a single molecule using SERS spectroscopy.[13,14] Regular assemblies of metal NPs are thus considered to be a useful platform for SERS devices.[15] One of the major difficulties in the practical application of SERS is the fabrication of subnanometer gaps in a controllable way.[16]

In the previous SERS reports[17,18] on the intracellular pH measurements, an individual metal NP (or aggregate) in the diameter range of 20−120 nm were endocytosized in a relatively freely diffusing condition without any spatial confinement. The distances among each NP are bound to change randomly via dynamic interactions with the cellular components. In particular, *in vivo* SERS experiments, NPs may be quickly either captured or cleared away via immune systems. All these intracellular changes may hamper reliable SERS measurement problematic by resulting in uncontrollable interparticle distances. While there has been an approach with improved molecular probes on NPs,[19] a new design of stable NP probe is highly desired. In this respect, controlled encapsulation of subnanogap-separated NP SERS probes via biocompatible materials will be highly beneficial to get more reliable intracellular pH measurements.

Biocompatible silica nanotubes (SNTs) have been currently utilized in spectral imaging.[20,21] Because of their void structures, SNTs may be applied to a vehicle for either magnetic or metal NP delivery system.[22] There has yet been no report on the subnanometer gap generation inside nanotubes for a SERS application.

In this work, we fabricated subnanometer gaps by encapsulating and closely packing *para*-mercaptobenzoic acid (*p*-MBA)-coated gold nanoparticles (AuNPs) with a mean diameter of ∼55 nm inside SNTs with an orifice diameter of ∼63 nm. Transmission electron microscopy (TEM) images clearly indicated that numerous junctions with the distance of subnanometer were formed among the AuNPs inside the SNTs. SERS spectra of *p*-MBA-coated AuNPs embedded in SNTs were found to change depending on the polarization angles with the evidence of single nanowire SERS. Despite several reports on the single nanowire SERS works,[23] there has not yet been a report on the single nanopeapod by introducing the analytes inside the nanotubes. Considering that dynamic interactions with surrounding constituents may induce phase transformations, energy exchange, and restructuring at the nanomaterial surfaces, either unintended aggregation or interparticle distance change in NPs may be avoided in our peapod system by encapsulating the nanogap-separated metal NPs inside silica tubes. Using these closely packed AuNP-embedded SNTs, we could develop a highly sensitive and well-protected single nanopeapod SERS sensor. The location of the AuNPs was controlled to be localized and closely packed inside the SNTs. These SNTPs can be utilized in advanced intracellular pH sensors.

■ EXPERIMENTAL SECTION

Materials. *N,N*-Diisopropylethylamine (DIEA, Aldrich, 99.5%), oleylamine (ACROS, 80−90%), gold(III) chloride hydrate (Aldrich, 99.999%), ammonium hydroxide (Daejung, 25−28%), tetraethyl orthosilicate (TEOS, Aldrich, 98%), aluminum foils (Alfa Aesar, 99.99%), *p*-mercaptobenzoic acid (*p*-MBA, Aldrich, 90%), oxalic acid (OCI company, 99.5%) and perchloric acid (70%, DC Chemical) were used as supplied without further purification.

Preparation of the AAO Templates. Alumina template was prepared according to the literature.[24] Briefly, preannealed aluminum foils (0.25 mm thick) were degreased in acetone for 1 h, and then electropolished at 5 °C and 15 V for 6 min in the mixed solution of perchloric acid and ethanol (volume ratio 1:5). The first anodization was performed in a 0.3 M oxalic acid solution for 10−15 h at 10 °C and 40 V, and then the resulting aluminum oxide layer was removed in a solution of phosphoric acid (6 wt %) and chromic acid (1.5 wt %) at 60 °C. To obtain AAO templates with either 500-nm or 1.7-μm pore

length, the etched aluminum foil was anodized again for 7 and 20 min, respectively. Finally, the pore diameters of the templates were controlled by the pore-widening times in phosphoric acid solution (5 wt %) at 30 °C. The pore-widening times for the AAO templates used to produce the SNTs with 63- and 74-nm orifice diameter were 29 and 32 min, respectively.

Preparation of SNTs. SNTs were prepared in the pores of the AAO template using sol−gel method according to the literature.[25] Typically, the template was soaked in a mixed solution of 95% ethanol, ammonium hydroxide, and TEOS (volume ratio 10:3:0.2) and allowed to react with stirring at room temperature for 28 min. After washing with ethanol several times, the template was cured in an oven at 120 °C for 15 min. The SNT-grown AAO template was then used to fabricate peapod structure containing AuNPs inside SNTs.

Preparation of AuNPs. AuNPs coated with hydrophobic capping agent was prepared according to the literature.[26] Briefly, a mixed solution of toluene and oleylamine (volume ratio 10:1) was refluxed for 1 h. HAuCl₄ (70 mg) dissolved in toluene and oleylamine (volume ratio 1: 1.2) was then injected to the above solution. The reaction mixture was heated for 1.5 h, and Au growth reaction was quenched by adding methanol. After collecting AuNPs by filtration, the samples were washed with methanol and redispersed in toluene. To obtain AuNPs of 35 and 55 nm diameter, the reaction cycles mentioned above were repeated three times and five times, respectively.

Fabrication of SNT Peapod (SNTP) Structure with AuNPs Inside. A piece of SNT-grown AAO template (SNT@AAO, 25 × 8 mm) was placed in a vacuum chamber on a rocking platform. To the surface of the template, a solution of AuNPs in toluene (4 mg/mL) was added dropwise until approximately a half of template's surface was covered with solution. Thereafter, the solvent was allowed to evaporate under vacuum condition with shaking at 35 rpm for 10 min. The SNT@AAO was then dried further in the oven at 40 °C and sonicated in toluene for 10 min to remove surface bound AuNPs rather than inserted in the pores of the SNTs. To obtain well-defined SNT peapod (SNTP) structure with AuNPs inside, the process mentioned above was repeated four times by a wet−dry process. Single-line linear chain AuNP SNTPs were obtained when 55-nm AuNP and SNT with 63 nm orifice diameter were used, whereas double-line linear chain AuNP SNTPs were obtained when 35-nm AuNP and SNT of 74 nm orifice diameter were used. For the control experiment, fused AuNPs inside SNT were separately prepared by calcining the AuNP-SNTPs at 350 °C for 3 h prior to *p*-MBA attachment process.

Fabrication of *p*-MBA-Attached SNTPs. The surface of AuNPs in SNTP was modified with *p*-MBA for SERS measurement by soaking the template obtained above in a solution of 0.1 M *p*-MBA in ethanol for 6 h. After drying in an oven at 40 °C, the template was cleaned by sonication in ethanol to remove the unreacted *p*-MBA inside SNTs. After silica layer on the surface of template was removed by mechanical polishing with aluminum oxide powder, the AAO template was dissolved in phosphoric acid (25 wt %) to obtain the free-standing *p*-MBA-attached AuNP-SNTPs. After collecting the SNTs by filtration, the final *p*-MBA-attached SNTP were washed with DI water several times and stored in DI water for the further use. The numbers of 1.7 μm length single- and double-line linear chain AuNP SNTPs were measured to be 3.6×10^{10} and 9.9×10^{10} mL^{-1}, respectively. The number densities of 500 nm length SNTs and AuNPs are 8.8×10^{8}/mL and 1.3×10^{10}/mL, considering that approximately 15 AuNPs are embedded inside each SNTP.

Physicochemical Characterization. The morphologies of SNTs were checked using a FEI TECNAI G2 transmission electron microscope (TEM). We checked the serum protein adsorption on *p*-MBA-coated AuNPs using a thermoelectron 6700 Fourier-transform infrared spectrometer with a nominal resolution of 4 cm^{-1} and 256 scanning times.

Cell Culture. Human leukemia K562 cells (ATCC CCL 243) and human lung carcinoma A549 cells (ATCC CCL-185) were cultured in RPMI 1640 medium supplemented with 10% fetal bovine serum (FBS) from WelGene (Seoul, Korea) and antibiotics at 37 °C in a 5% CO₂ atmosphere incubator.

TEM Images of Cellular Uptake of SNTPs. The uptake of NPs was examined using a JEOL 1010 TEM. Ultrathin sections for TEM were prepared with a diamond knife to be analyzed.

Dark-Field Microscopy (DFM). Cellular uptake of NPs was also monitored using dark-field microscopy with a Leica DL LM upright microscope and a high-resolution Cytoviva (Auburn, USA) 150 adapter.

Surface-Enhanced Raman Scattering (SERS). By dropping the solution to the SiO₂ surfaces, we can find a single nanopeapod. SERS spectra were obtained using a Raman confocal system model 1000 microscope spectrometer (Renishaw) equipped with an integral microscope (Leica DM LM) and polarizer at the excitation wavelength of 632.8 nm.

***In Vivo* SERS Spectra.** Six week old male CAnN.Cg-Foxn1nu/CrljOri nude mice (Orient Bio, Inc., Gyeonggi, Korea) were used for *in vivo* SERS measurements. All animal experiments were performed in compliance with the guidelines of the Institute of Laboratory Animal Resources, Seoul National University (SNU-101221-1).

■ RESULTS AND DISCUSSION

Figure 1 shows a schematic diagram for the preparation of nanopeapod structure based on AuNPs and SNTs via solvent
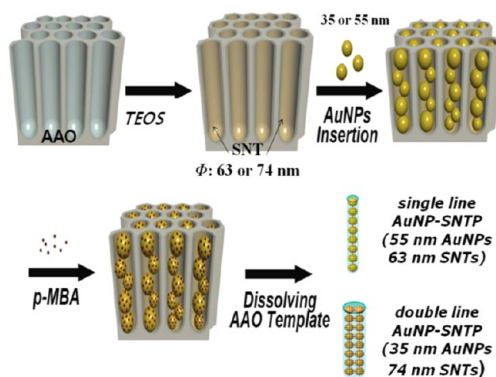

Figure 1. Synthetic scheme of either a single-line or a double-line linear AuNP chain nanopeapod. Generation of well-preserved subnanometer gaps among the closely packed AuNPs inside the SNTPs by self-assembly.

evaporation assisted capillary force.[27] To the surface of SNT-grown AAO template, a solution of AuNPs dispersed in toluene was added. The solvent was then allowed to be evaporated *in vacuo* on a rocking platform. For SERS measurement, *p*-MBA was assembled on the AuNPs in SNTP before dissolving the AAO template. After dissolving the AAO template in phosphoric acid, the free-standing SNTPs were collected by filtration and stored in DI water for the further use.

Figure 2 shows TEM images of SNTP prepared from different sets of AuNP and SNT combinations. SNTPs consisting of well-defined single-line linear AuNPs inside SNTs were obtained, when relatively larger AuNPs (~55 nm) and SNTs with narrower pore diameter (~63 nm) were used (Figure 2a,b; Figures S1 and S2, Supporting Information). In contrast, SNTPs with double-line AuNPs inside SNTs were obtained by using smaller AuNPs (~35 nm) and wider SNTs (~74 nm) (Figure 2c,d; Figures S3 and S4, Supporting Information). This reveals that the geometry of nanopeapod structure can also be controlled by the size of AuNPs and inner diameter of SNTs used in the insertion experiment.

Judging from TEM images of SNTP (Figure 2b,d), it is noticeable that the gap distances between AuNPs are as short as subnanometer range, where the strong Raman enhancements
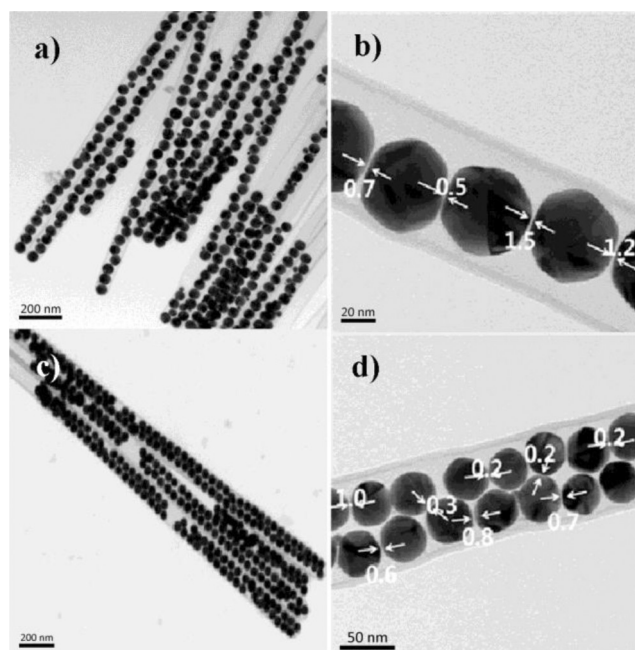

Figure 2. Representative TEM images of free-standing single-line (a, b) and double-line (c, d) linear AuNP chain SNTP with a length of 1.7 μm. Magnified view where the distances between the AuNPs are recorded as subnanometer gaps, some of which may generate hot spots in the picture.

are expected. As anticipated, the values obtained from TEM measurement may not reflect the real gap distances because these values can be varied when observing angle is not perpendicular to the gap formed by AuNPs. Nonetheless, more intense works on gap distance measurement carried with 50 different SNTPs revealed that nanogap junctions with a distance of the subnanometer gaps were formed among AuNPs inside SNTPs (Table S1, Supporting Information). Our measurements could not exactly depict the three-dimensional configurations of AuNPs inside SNTS. The accuracy of the interparticle spacing between TEM measurements would be 10−20%. The average numbers of AuNPs inside a SNT were ~30 and ~90, for the 1.7 μm long single-line and double-line SNTPs, respectively (Table S2, Supporting Information).

Figure 3 illustrates a plausible mechanism for controlled AuNP close-packing in SNTs by solvent evaporation assisted capillary forces.[27] This plays a critical role in preparation of well-defined peapod structure, creating continuous and repeating wet−dry condition to the interface between the inner wall of SNTs and AuNP solution. More detailed mechanism for the formation of closely packed NPs in SNTs is under investigation.

As shown in Figure 4, to predict the electromagnetic enhancements from the nanogap junctions in SNTPs, we performed FDTD calculations[28] for single-line and double-line SNTPs. Calculated near-field electromagnetic field distribution of the AuNPs inside SNTs indicated strong electric field enhancement. The light is incident along the direction perpendicular to the long axis of silica tube. In our peapod system, the light polarized at 0° would have favorable excitation along with the nanotube long axis. For the polarization parallel to the long axis of silica tube, the single-line AuNP chain SNTPs exhibited up to a 3.0×10^4 enhancement of $|(E^2)|$. If the
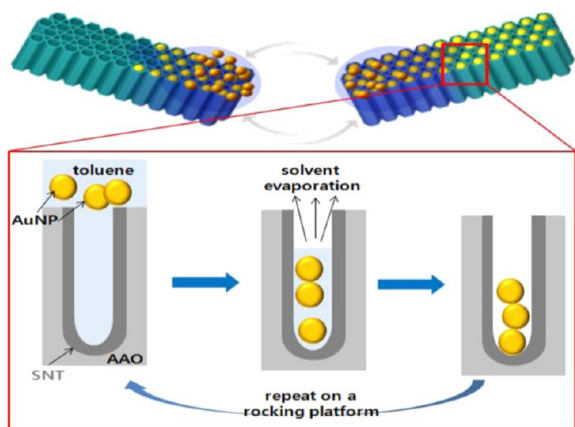
Figure 3. A proposed mechanism for controlled AuNP close-packing in SNTs by solvent evaporation assisted capillary forces.
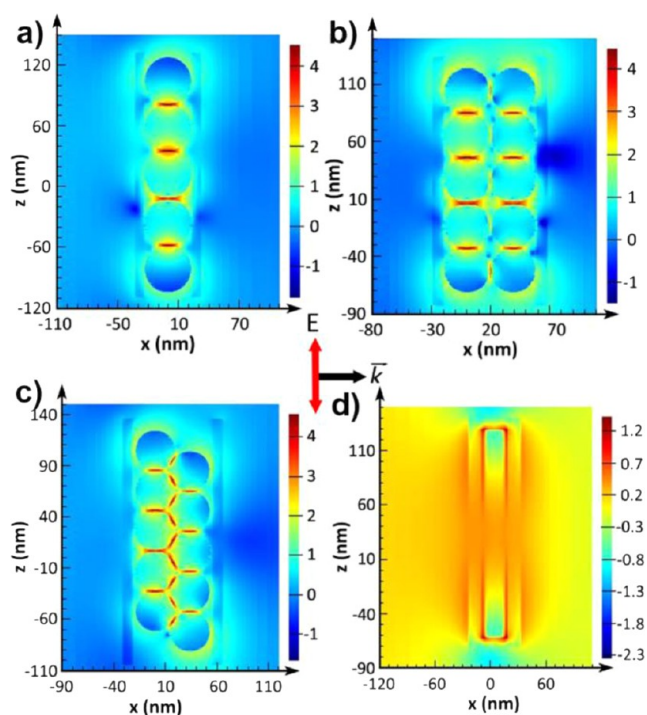

Figure 4. Finite dimension time domain (FDTD) calculations of (a) single-line linear, (b) double-line linear, (c) double-line zigzag AuNP-encapsulated SNTPs, and (d) a fused cylinder sample. The different colors indicated the calculated near-field electromagnetic field distribution (E^2) of the AuNPs inside the SNTPs excited at 632.8 nm. The gap distances are assumed to be 0.9 nm. The E and k vectors indicate the incident direction of laser light and the polarization, respectively. The color bar represents the value of $\log(E/E_o)^2$.

polarization is perpendicular to the long axis of silica tube, the enhancements are reduced to be only 21 times. For comparison, double-line AuNP chain SNTPs showed the maximum 2.8×10^4 enhancement. It has to be mentioned that there are nanogap junctions perpendicular to the long axis of silica tube for the double-line SNTPs. When the polarization is at 45° with respect to the long axis of silica tube, the double strand zigzag line and the cylindrical shape of AuNPs show the maximum enhancements of 1.2×10^4 and 70, respectively. If the polarization is perpendicular to the long axis of silica tube, the enhancements are reduced to be only 15 and 60. If the AuNPs are fused into a cylinder, only a 24 time enhancement is

expected. The Au cylinder without any nanogaps exhibited only a small enhancement in electric field.

To assess the performance of SNTPs as a single nanopeapod sensor by means of Raman spectroscopy, we obtained the polarized response of single nanopeapod embedded with linearly aligned AuNPs having nanometer gap distances. AuNPs were closely packed with the bifunctional linker *p*-MBA. The optical image of single-line SNTPs was illustrated (Figure S5, Supporting Information) along with the experimental setup (Figure S6, Supporting Information). The strong SERS bands at 1080 and 1590 cm^{-1} clearly indicated the *p*-MBA peaks assembled on AuNPs (Figure 5). As shown in
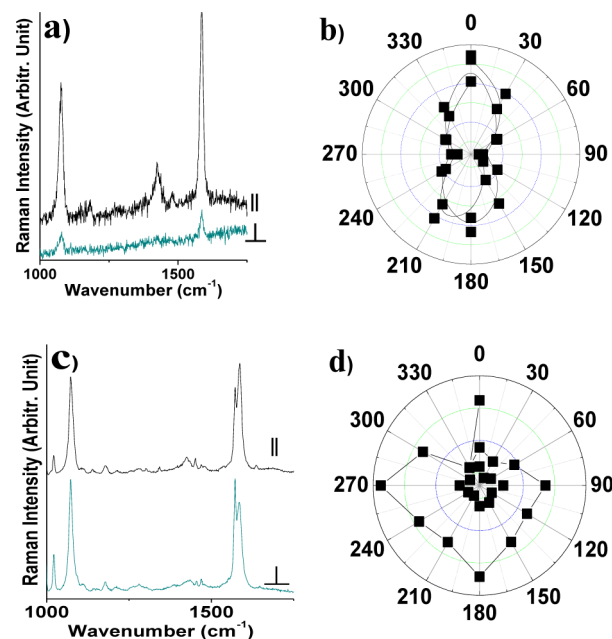

Figure 5. Single nanopeapod SERS spectra. (a) SERS spectra of *p*-MBA of single-line linear AuNP chain SNTs and (b) its polar plots of the SERS intensity, which could be fitted as a cosine-squared function. The Raman band intensities at 1590 cm^{-1} of *p*-MBA were measured as a function of polarization angle. (c) SERS spectra of *p*-MBA of doubly aligned SNTPs. (d) Polar plots of the SERS intensity of double-line linear AuNP chain SNTP. Stronger SERS intensities for the double-line SNTPs were presumably due to the larger orifice diameters of the SNTs and the greater number of AuNPs than those of the single-line SNTPs.

Figure 5a, we could observe the spectra change. The aromatic ring and antisymmetric carboxylate band at 1080, 1590, and 1427 cm^{-1} became significantly reduced at the perpendicular polarization angles. The intensity at 0° was observed to be larger than that at 90°. On the other hand, we could not observe any polarization dependence for the doubly aligned AuNP SNTPs as shown in Figure 5b. Please note that the nanogaps are formed vertically for the parallel shape as well as horizontally. This makes the polarization dependence vanish, differently from the case of single-line AuNP chain SNTP. Using the subnanometer gap-generated AuNP-embedded SNTP, we could develop a reliable Raman sensor that is separated from the outer environment by silica walls. Our nanopeapod system can be potentially applied to develop polarizer components in nanoscale sensors. The doublet SERS peaks at 1570 cm^{-1} along with 998 and 1020 cm^{-1} can be ascribed to the thiophenol peaks.[10c] A part of the *p*-MBA

adsorbate may be decomposed to the thiophenol on metal surfaces. The reason why we could not observe the thiophenol peaks on the single line may be due to their weak signal-to-noise ratios. In fact the double line intensities appeared to be 20 times stronger than those of the single line SNTPs. On the other hand, we could observe the thiophenol peaks along with the doublet peak at 1575 cm^{-1}, even for the single-line SNTPs inside cell (Figure S7, Supporting Information).

We attempted to apply our SNTPs for the practical purpose. To demonstrate SNTP-based pH nanosensors working inside cells, 500-nm SNTPs with double line AuNP array inside and their control without hot spots were fabricated. For more efficient cellular delivery, shorter lengths of SNTP were fabricated with slightly different dimensions (Figure S8, Tables S3 and S4, Supporting Information). Figure 6a shows the TEM
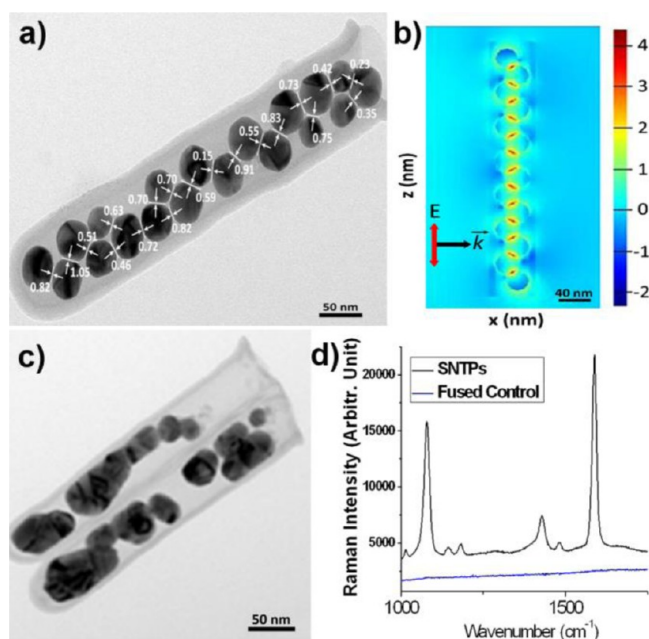

Figure 6. (a) TEM image of a free-standing nanogap-fabricated AuNP-embedded SNTP with a length of 500 nm. The nanogap fabrication is indicated by the two arrows. The recorded distances between the AuNPs showed that subnanometer gaps of ∼0.9 nm were formed to generate the subnanometer gaps shown in the image. (b) FDTD calculations of electric field enhancements |(E²)| of the SNTPs. The zigzag shape and double line identify the AuNP-encapsulated SNTPs. The average AuNP diameter and the orifice diameter of SNTs are measured to be ∼36 and ∼55 nm, respectively. (c) TEM image of fused control. (d) SERS spectra of the 500 nm SNTPs and fused control.

image of a free-standing nanogap-separated AuNP-embedded SNTP. The gap distances between AuNPs were measured to be ∼0.9 nm. Figure 6b shows the FDTD calculations of the electric field enhancements between the nanogaps.[28]

As shown in Figure 6b, our FDTD calculations indicate strong electromagnetic enhancements for the nanogaps of AuNPs inside SNTP. As a control experiment, we fabricated the fused control separately by calcining AuNP-SNTP at 350 °C. Figure 6c shows the TEM image of the fused control containing linear cylinder type fused Au inside SNTs without any nanogap. As we mentioned earlier, the presence of nanogap in SNTP can be proved by enhancement of SERS signal of p-MBA assembled on AuNP-SNTP. Figure 6d shows SERS

spectra of nanogap-fabricated AuNP-SNTP and fused control. As anticipated, the strong SERS bands at 1076 and 1590 cm^{-1} were clearly detected in case of p-MBA attached AuNP-SNTP, whereas no SERS peaks were observed for the controlled fused particles. This indicates that the nanogaps observed and assigned in TEM analysis are valid and in accordance with the SERS measurements. The SERS intensities were greatly enhanced for the AuNPs closely packed inside SNTP, whereas the control sample did not exhibit any Raman enhancements.

For the thiol monolayer coverage, 0.216 nm^2 for each adsorbate occupied the surface area of a single AuNP with radius R being $4\pi R^2$ ($4\pi \times 18.2^2 = 4.16 \times 10^3$ nm^2). Assuming that 1.92×10^4 p-MBA molecules can adsorb on each AuNP surface, the concentration of p-MBA in SNTP is estimated to be 2.5×10^{14}/mL ∼ 0.40 μM. The enhancement factors may be estimated as the following formula:

$$(\text{enhancement factor}) = (I_{\text{SERS}}/I_{\text{bulk}}) \times (N_{\text{bulk}}/N_{\text{SERS}})$$

By comparing the ordinary Raman intensity of p-MBA in 1 M and assuming the number of p-MBA molecules in SNTP to be 0.40 μM, the enhancement factor can be estimated to be 3.1 × 10^7. This is not such a great enhancement as the organic dye, but sufficient to observe the single nanopeapod sensitivity under our experimental conditions.

Since AuNPs were internally well-stabilized to have subnanometer gaps with a fixed distance inside SNTs, this SNTP system was expected to produce a consistent SERS signal. The SERS spectra of p-MBA-coated AuNPs embedded in SNTPs were found to change, depending on pH values. After the endocytosis of p-MBA-coated AuNP-embedded SNTPs in mammalian cells, intracellular pH values could be examined in a successful way. The H$^+$ ions are assumed to shuttle through both the orifices and side walls of SNTs from the previous report of the silica-etching using a strong acid.[29]

As shown in Figure 7, we could observe the spectra change. At pH 5, the symmetric carboxylate band at ∼1423 cm^{-1}
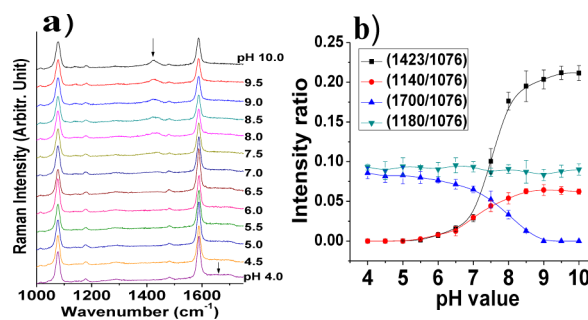

Figure 7. (a) SERS spectra of the 500 nm SNTPs at different pH values from 4 to 10. The arrow indicates the pH-sensitive carboxylate symmetric stretching-related bands at 1140 and 1423 cm^{-1} in the pH-sensitive band region of 1100−1500 cm^{-1}. Please note that the band at 1180 cm^{-1} did not change much, whereas the other band at 1423 cm^{-1} changed sensitively as marked with arrow. (b) pH calibration curves for the four bands.

became significantly reduced. The weaker band at ∼1140 cm^{-1} also showed similar behavior. The relative intensities of the carboxylate band at ∼1423 cm^{-1} with respect to one of the strongest aromatic ring modes at ∼1076 cm^{-1} was plotted. Besides the 1423 cm^{-1} band (the symmetric carboxylate stretching: $\nu(\text{COO}^-)$), the 1140 cm^{-1} (mixed mode) also decreased at low pH values. On the other hand, when the pH

values became acidic, then the 1700 cm^{-1} band (the carbonyl stretching mode: $\nu(C=O)$) increased in intensity due to the protonation of the carboxylate group. These bands may be a good indicator of a pH change from the neutral to the acidic compartments. Considering that the endosomal and lysosomal pH values are 5.5 and 4.5, respectively, we could judge the intracellular localization of SNTP. As in the case of Figure 7a, at pH 5, the antisymmetric carboxylate band at ~1423 cm^{-1} became significantly reduced. Given the other SERS peaks appeared to be analogous to the previous report.[17,18] Gold nanoaggregates attached to aromatic adsorbates enable biocompatible pH probing, based on SERS signals for live cell studies.[30] One of the disadvantages of conventional plasmonic biosensors is that metal NPs are bound to be directly exposed to the biological milieu and severely interfered by intracellular constituents, since NPs interacting with proteins, membranes, cells, DNA, and organelles create NP/biological interfaces that depend on colloidal forces and dynamic chemical interactions.[31] These interactions are known to lead to the formation of protein coronas, particle wrapping, and biocatalytic processes resulting in unexpected and irregular particle aggregations. Adsorbed biomolecules may induce phase transformations, energy exchange, and restructuring at the nanomaterial surface to change the interparticle distances. Intracellular compartments and cell culture media may contain interfering biomolecules including gold-binding proteins. Under these circumstances, it is imperative to provide a consistent and well-confined environment for AuNPs in order to measure intracellular pH values.

Regarding the pH calibration curves, the change occurs in an acidic region. Although the pKa value[32] of *p*-MBA is estimated to be 6.81 and the *p*-MBA molecules are expected to become slightly basic in the cellular medium of neutral pH values of 7−8, the value on the surface may be changed more in surface states than in the solution state. Our SERS spectra indicated that the weak bands at 1423 and 1140 cm^{-1} almost disappeared at pH values below pH 5. This suggests that the band analysis using only ~1423 cm^{-1} may be not very efficient at acidic pH values. By using the carbonyl peak bands at ~1700 cm^{-1} which became intensified under acidic conditions, better pH estimation should be possible in combination with the carboxylate stretching bands.

A pH nanosensor reporting enhanced intracellular SERS after the endocytosis of *p*-MBA-coated AuNP-embedded SNTs in mammalian cells would be one of the ideal bioapplications which we could develop based on the SNTP. First we attempted to find a pH sensor application by obtaining SERS spectra of *p*-MBA at different pH values. To examine whether SNTP can be utilized as a nanosensor, we obtained Raman spectra. As shown in Figure 7, the strong SERS bands at 1076 and 1590 cm^{-1} clearly indicated the pH-sensitive *p*-MBA peaks from AuNPs.

We are currently working on the colocalization of DFM and lysosomal overlaid images. After excluding the possibility of SNTPs in lysosomes, where the pH values are quite acidic to be 4.5−5.5, the intracellular pH values could be better estimated in the neutral or slightly alkaline region. In addition, we are planning to use *para*-aminobenzenethiol[33] and *ortho*-mercapto-benzoic acid[34] adsorbates on AuNPs, which may overcome the weakness of the SERS peaks in acidic regions.

Our study indicated SNTPs were well internalized inside mammalian cells, as shown in the TEM image of Figure 8a,b. It is noteworthy that the nanogaps were preserved inside the cells.
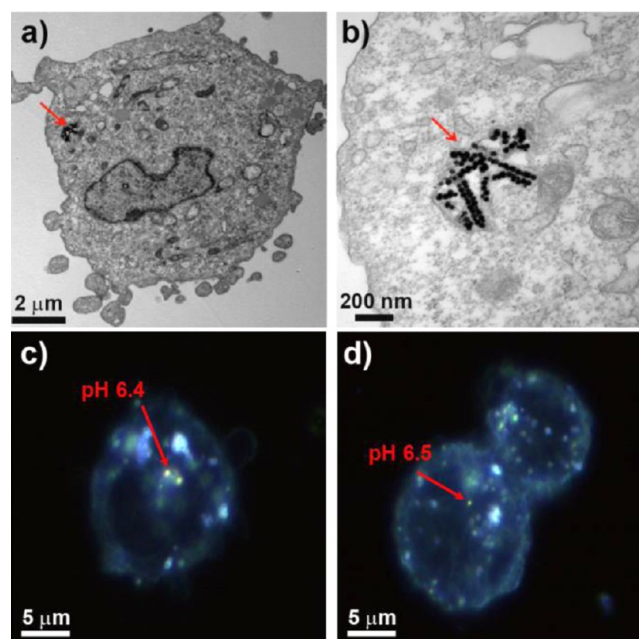

Figure 8. TEM images (a, b) of SNTPs in K562 cells. The right picture is a magnified view of the left one. The arrow indicates the location of SNTPs. Nanogap distances appeared to be well sustained inside the SNTPs. (c, d) pH values based on the band intensities at ~1423 cm^{-1} at the places pointed by the arrows in the dark-field microscopy (DFM) images of K562 mammalian cells.

Moreover, SERS signals could be monitored to estimate the pH values by using the maintained nanogap distances, after endocytosis of the SNTP. To further examine the possibility of an intracellular pH sensor, we performed a combined study of dark-field microscopy and SERS after incubation of SNTPs into mammalian cells as illustrated in Figure 8c,d.

As presented in Figure 8c, we could estimate the pH values by observing the spectral difference at various positions of intracellular compartments. In quite a few spots, the SERS spectra indicated fairly pH sensitive behaviors. The neutral pH positions could be found at either cell surfaces or extracellular parts. We tested different cell lines of A549 cell lines and obtained similar results (Figure S9, Supporting Information). It was found that the SNTPs were well-endocytosed and located inside either lysosomes or endosomes.

Our infrared measurements, the serum proteins were adsorbed on bare AuNPs without SNT encapsulation by identifying the protein amide bands (Figure S10, Supporting Information). We checked the stability of Raman sensors for *p*-MBA-coated AuNPs after an equal volume treatment of the cell culture Roswell park memorial institute (RPMI) medium (10% mixture). As suggested from the infrared spectra, it is possible that there is a dynamic protein-AuNP interaction in cellular media for the pH-sensing MBA of the short aromatic thiol compounds. This limitation can prevent detection of any pH measurements in a local area of cellular compartments. Our SNTPs could be used to develop a highly sensitive advanced sensor. Considering that cells and cell-culturing media contain a variety of proteins, lipids, and other constituents and that Raman signals are ultrasensitive to hot-spot formation, it should be advantageous if the generated nanogaps are well-arrayed despite the dynamic biophysicochemical interactions.

While it is not clear if those encapsulated SNTPs are in endosome or lysosome based on TEM images (Figure S11,

Supporting Information), considering that most of measured pH values are around 6, most of SNTPs may be in early endosomal encapsulation or escaped into cytosol, not in lysosome. However, these internalization mechanisms should be investigated further for clear conclusion. We are currently doing colocalization study of endocytosis process over time correlating with SERS signals.

We used equal concentrations (1.3×10^{10}/mL) of AuNPs without any SNT encapsulation and found that the SERS intensities appeared to be much weaker (Figure 9). After
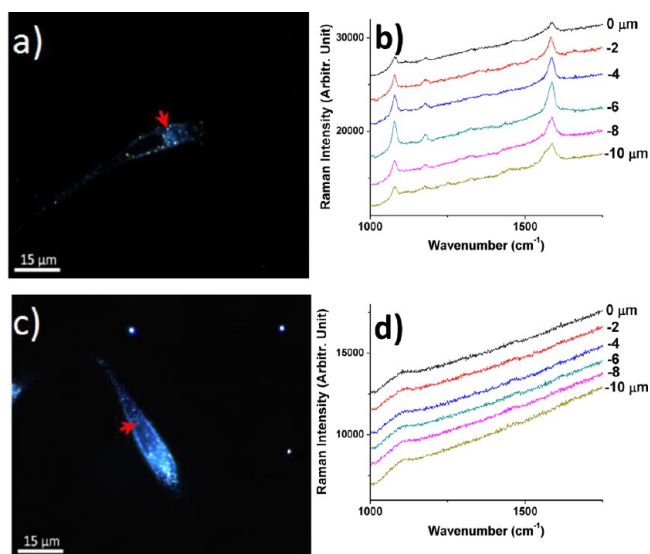

Figure 9. Comparative SERS spectra for relative intensities of SNTPs and AuNPs with an equal number of AuNPs (1.3×10^{10}/mL). (a) DFM image and (b) the corresponding SERS spectra marked with an arrow for the SNTPs. (c) DFM and (d) Raman spectra of AuNPs without any encapsulation of SNTs in A549 cells with an equal number of AuNPs in a single A549 cell. SNTPs were supposed to be located 6 μm below the bottom of the cover glass, where the strongest SERS were observed. On the other hand, the SERS spectra were not well observed without SNT encapsulation.

applying the sample to A549 cancer cells, we could find the strong SERS intensities easily for SNTPs, whereas the AuNP sample was barely observable, if the equal amount of AuNPs were used without SNT encapsulation.

We compared the SERS spectra with or without any SNT encapsulations and found that the relative fluctuations of intensity variations could be reduced for the SNTPs (Figures S12 and S13, Supporting Information). The relative intensities of 20 different SNTPs are within 15%, whereas that of AuNPs revealed quite random distributions as high as 46%. Moreover, the selected 500 nm SNTPs showed the intensity variations as low as 10% due to their smaller number of nanogap junctions by smaller number of AuNPs than the case of the 1.7 μm SNTPs. We have to mention that only the 500 nm SNTPs were used for the intracellular pH measurements. Considering that one of the main difficulties presented in the earlier work is the large variation in the pH response from one particle to another due to uncontrolled aggregation of AuNPs inside cells. Our data suggest that SNTPs provide an improved method in comparison with only AuNP aggregates[30] in terms of reliability and reproducibility of pH measurements. Along with the lower amount of AuNP usages by the SNTP encapsulation as demonstrated in Figure 9, our SNTP method may provide

improved spectral quality due to the confinement of AuNPs inside SNTs. The nanogap distributions range from 0.2 to 1.3 nm (Figure S14, Supporting Information). Each individual 500 nm SNTP has 8−15 nanogaps with their average values reduced to 0.6−1.3 nm. Since single SNTP may have relatively uniform distributions, the fluctuation may be averaged out considerably. The nanogaps of SNTPs were measured to be in the range of 0.6−1.3 nm of which variations may affect the SERS intensity.

To check the interference from the other ions, we used potassium and sodium buffer solutions at the concentrations of 1, 10, 100 mM, which are commonly used in the physiological conditions. We found that the relative SERS intensity ratios did not change significantly even in the presence of the other monocations such as K$^+$ and Na$^+$ in their physiological concentrations of 1−100 mM (Figures S15 and S16, Supporting Information). These results suggest that our methods can be applied with the two representative physiological monocations.

The current pH fluorescence microprobes have several disadvantages of photobleaching (Figures S17 and S18, Supporting Information). By irradiating the laser for a few minutes, the fluorescence signals disappeared considerably. In comparison with these fluorescence probes, our SERS methods have several advantages of long-time monitoring.

We have tested spectra behaviors for the *in vivo* usages to examine the benefit of SNTP encapsulations. Figure 10
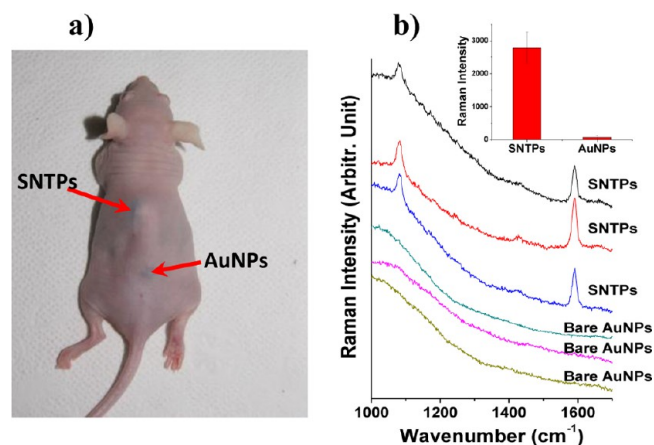

Figure 10. *In vivo* SNTP sensor. (a) Photograph of the injected site. (b) SERS spectra of SNTPs and bare AuNPs coated with *p*-MBA. We checked that both the two samples of SNTPs and bare AuNPs produced strong SERS signal prior to the subcutaneous injections. Three independent measurements were performed to give the average values and error bars of the inset bar chart.

compares the SERS intensities of only bare AuNPs and SNTPs. It was found that the SERS intensities of the silica-encapsulated AuNPs exhibited much higher intensities than the case of only AuNPs were used. In fact, if only AuNPs were injected subcutaneously without silica encapsulation, we could not find any strong SERS intensities of *p*-MBA. This may be due to less clearance of SNTPs because of their biocompatibility of silica materials. We concluded that AuNPs without silica encapsulation are supposed to be either cleared fast or diffused away without maintaining the nanogap distances. In this respect, our SNTPs can provide well-sustainable subnanometer gaps for an advanced pH sensor both *in vitro* and *in vivo*.

CONCLUSIONS

We fabricated either a single-line or a double-line linear AuNP chain silica peapod by controlling the orifice and the NP diameters. The TEM images indicated numerous nanogap junctions with distances of more or less than 1 nm were formed between the AuNPs inside the SNTs. It was only for the single-line SNTPs that the SERS spectra of p-MBA in SNTs were found to change depending upon the polarization angles. The TEM images indicated that the AuNPs inside the SNTPs appeared to have a well-preserved geometry from the cellular environments in the presence of the interference from the biological ingredients. The SERS spectra of p-MBA in SNTP changed, depending upon the pH values. Intracellular pH values could be examined after the endocytosis of p-MBA-coated AuNP-embedded SNTPs in mammalian cells. SNTPs exhibited superior quality surface-enhanced Raman scattering (SERS) spectra in vivo due to well-sustained nanogap junctions inside the SNTs, when compared to simply using AuNPs without any silica encapsulation. In addition, we demonstrated that less fluctuation of SERS intensity variations for SNTPs resulted in more reliability and reproducibility of pH measurements with less usage of AuNPs. Although the peapod structure control of SNTPs still leaves room for improvement, it is expected that a robust intracellular optical pH sensor could be developed with the advantage of the sustained nanogaps by using the SNTPs.

ASSOCIATED CONTENT

Ⓢ Supporting Information

Detailed experimental data, TEM images of SNTPs, size distributions, and high-resolution TEM, DFM, polarized Raman results, doublet feature of single-line SNTPs, SERS spectra of 20 SNTPs and AuNP aggregates, interference test of K^+ and Na^+, and fluorescence probe test. This material is available free of charge via the Internet at http://pubs.acs.org.

AUTHOR INFORMATION

Corresponding Author

sjson@gachon.ac.kr; slee@umd.edu; sjoo@ssu.ac.kr

Notes

The authors declare no competing financial interest.

ACKNOWLEDGMENTS

REFERENCES

(1) (a) Henzie, J.; Andrews, S. C.; Ling, X. Y.; Li, Z.; Yang, P. *Proc. Natl. Acad. Sci. U. S. A.* **2013**, *110*, 6640−6645. (b) Slaughter, L. S.; Willingham, B. A.; Chang, W.-S.; Chester, M. H.; Ogden, N.; Link, S. *Nano Lett.* **2012**, *12*, 3967−3972. (c) Hu, M.; Ou, F. S.; Wu, W.; Naumov, I.; Li, X.; Bratkovsky, A. M.; Williams, R. S.; Li, Z. *J. Am. Chem. Soc.* **2010**, *132*, 12820−12822.

(2) Yao, Y.; Chaubey, G. S.; Wiley, J. B. *J. Am. Chem. Soc.* **2012**, *134*, 2450−2452.

(3) (a) Gunawidjaja, R.; Kharlampieva, E.; Choi, I.; Tsukruk, V. V. *Small* **2009**, *5*, 2460−2466. (b) Barrow, S. J.; Funston, A. M.; Gómez, D. E.; Davis, T. J.; Mulvaney, P. *Nano Lett.* **2011**, *11*, 4180−4187. (c) Lee, D.; Choe, Y.-J.; Choi, Y. S.; Bhak, G.; Lee, J.; Paik, S. R. *Angew. Chem., Int. Ed.* **2011**, *50*, 1332−1337. (d) Kolb, F. M.; Berger, A.; Hofmeister, H.; Pippel, E.; Gösele, U.; Zacharias, M. *Appl. Phys. Lett.* **2006**, *89*, 173111.

(4) Hunyadi, S. E.; Murphy, C. J. *J. Phys. Chem. B* **2006**, *110*, 7226−7231.

(5) Wustholz, K. L.; Henry, A.-I.; McMahon, J. M.; Freeman, R. G.; Valley, N.; Piotti, M. E.; Natan, M. J.; Schatz, G. C.; Van Duyne, R. P. *J. Am. Chem. Soc.* **2010**, *132*, 10903−10910.

(6) Cecchini, M. P.; Wiener, A.; Turek, V. A.; Chon, H.; Lee, S.; Ivanov, A. P.; McComb, D. W.; Choo, J.; Albrecht, T.; Maier, S. A.; Edel, J. B. *Nano Lett.* **2013**, *13*, 4602−4609.

(7) Aćimović, S.; Kreuzer, M.; Gonzáez, M.; Quidant, R. *ACS Nano* **2009**, *3*, 1231−1237.

(8) Xu, J.; Zhang, L.; Gong, H.; Homola, J.; Yu, Q. *Small* **2011**, *7*, 371−376.

(9) Hao, E.; Schatz, G. *J. Chem. Phys.* **2004**, *120*, 357−366.

(10) (a) Lee, S. J.; Baik, J. M.; Moskovits, M. *Nano Lett.* **2008**, *8*, 3244−3247. (b) Ou, F. S.; Hu, H.; Naumov, I.; Kim, A.; Wu, W.; Bratkovsky, A. M.; Li, X.; Williams, R. S.; Li, Z. *Nano Lett.* **2011**, *11*, 2538−2542. (c) Michota, A.; Bukowska, J. *J. Raman Spectrosc.* **2003**, *34*, 21−25.

(11) Cialla, D.; März, A.; Böhme, R.; Theil, F.; Weber, K.; Schmitt, M.; Popp, J. *Anal. Bioanal. Chem.* **2012**, *403*, 27−54.

(12) Gordon, R.; Sinton, D.; Kavanagh, K. L.; Brolo, A. G. *Acc. Chem. Res.* **2008**, *41*, 1049−1057.

(13) Nie, S.; Emory, S. *Science* **1997**, *275*, 1102−1106.

(14) Kneipp, K.; Wang, Y.; Kneipp, H.; Perelman, L.; Itzkan, I.; Dasari, R.; Feld, M. *Phys. Rev. Lett.* **1997**, *78*, 1667−1670.

(15) Rao, C. N. R.; Kulkarni, G. U.; Thomas, P. J.; Edwards, P. P. *Chem. Soc. Rev.* **2000**, *29*, 27−35.

(16) Chen, A.; DePrince, A. E., III; Demortiere, A.; Joshi-Imre, A.; Shevchenko, E. V.; Gray, S. K.; Welp, U.; Vlasko-Vlasov, V. K. *Small* **2011**, *7*, 2365−2371.

(17) Talley, C. E.; Jusinski, L.; Hollars, C. W.; Lane, S. M.; Huser, T. *Anal. Chem.* **2004**, *76*, 7064−7068.

(18) Kneipp, J.; Kneipp, H.; Wittig, B.; Kneipp, K. *J. Phys. Chem. C* **2010**, *114*, 7421−7426.

(19) Lawson, L.; Huser, T. *Anal. Chem.* **2012**, *84*, 3574−3580.

(20) Jammaer, J.; van Erp, T. S.; Aerts, A.; Kirschhock, C. E.; Martens, J. A. *J. Am. Chem. Soc.* **2011**, *133*, 13737−13745.

(21) Hillebrenner, H.; Buyukserin, F.; Stewart, J. D.; Martin, C. R. *Nanomedicine* **2006**, *1*, 39−50.

(22) Son, S. J.; Reichel, J.; He, B.; Schuchman, M.; Lee, S. B. *J. Am. Chem. Soc.* **2005**, *127*, 7316−7317.

(23) Fazio, B.; D'Andrea, C.; Bonaccorso, F.; Irrera, A.; Calogero, G.; Vasi, C.; Gucciardi, P. G.; Allegrini, M.; Toma, A.; Chiappe, D.; Martella, C.; Buatier de Mongeot, F. *ACS Nano* **2011**, *5*, 5945−5956.

(24) Mitchell, D. T.; Lee, S. B.; Trofin, L.; Li, N.; Nevanen, T. K.; Soderlund, H.; Martin, C. R. *J. Am. Chem. Soc.* **2002**, *124*, 11864−11865.

(25) Jayaraman, K.; Okamoto, K.; Son, S. J.; Luckett, C.; Gopalani, H.; Lee, S. B.; English, D. S. *J. Am. Chem. Soc.* **2005**, *127*, 17385−17392.

(26) Hiramatsu, H.; Osterloh, F. E. *Chem. Mater.* **2004**, *16*, 2509−2511.

(27) (a) Liddle, J. A.; Cui, Y.; Alivisatos, P. *J. Vac. Sci. Technol., B: Microelectron. Nanometer Struct.—Process., Meas., Phenom.* **2004**, *22*, 3409−3414. (b) Krachevsky, A.; Nagayama, K. *Adv. Colloid Interface Sci.* **2000**, *85*, 145−192.

(28) *FDTD Solutions 6.5*; Lumerical Solutions, Inc.: Vancouver, BC; http://www.lumerical.com/ftdt.php.

(29) Dean, S. L.; Stapleton, J. J.; Keating, C. D. *Langmuir* **2010**, *26*, 14861−14870.

3840

dx.doi.org/10.1021/ja411034q | *J. Am. Chem. Soc.* 2014, 136, 3833−3841

(30) Wang, F.; Widejko, R. G.; Yang, Z.; Nguyen, K. T.; Chen, H.; Fernando, L. P.; Christensen, K. A.; Anker, J. N. *Anal. Chem.* **2012**, *84*, 8013−8019.

(31) Nel, A. E.; Mädler, L.; Velegol, D.; Xia, T.; Hoek, E. M.; Somasundaran, P.; Klaessig, F.; Castranova, V.; Thompson, M. *Nat. Mater.* **2009**, *8*, 543−557.

(32) Smith, R.; Martell, A. E. *The Critical Stability Constant Database, NIST Standard Reference Database*; NIST: Washington, D.C., 1993.

(33) Wang, F.; Widejko, R. G.; Yang, Z.; Nguyen, K. T.; Chen, H.; Fernando, L. P.; Christensen, K. A.; Anker, J. N. *Anal. Chem.* **2012**, *84*, 8013−8019.

(34) Lee, S. B.; Kim, K.; Kim, M. S. *J. Raman Spectrosc.* **1991**, *22*, 811−817.